INTERNATIONAL JOURNAL OF
NUMERICAL ANALYSIS AND MODELING
Volume 13, Number 2, Pages 220–229

AN IMMERSED BOUNDARY METHOD FOR DIATOM SEDIMENTATION

YU-HAU TSENG, PING HUANG, AND HUAXIONG HUANG

Abstract. We propose a mathematical model and immersed boundary method for the growth and breakup of diatom chains. Diatom chains are treated as zero thickness open curves thanks to their small aspect ratio. The growth of the chain is modelled by adding small pieces of diatoms at the two end points while the breakup is done by removing a small piece in the middle of the chain. Numerical experiments are carried out to investigate the effects of growth and breakup on the sedimentation rate of diatom chains. Simulations of multiple diatom chains show that sedimentation rate is highly dependent on diatoms' spatial distribution. The results can be used to explain the observations that diatoms often form chain-like structures in natural habitats.

Key words. Diatom sedimentation, hydrodynamic interaction, immersed boundary method.

1. Introduction

In many taxonomic groups, colony formation among planktonic organisms suspended in water is very common. The colonial structures are formed in many ways and many colonies take the form of chains [14]. Diatom is one of the most important species among those phytoplankton [1]-[3]. It is found that diatoms are capable of existing as independent units and also join together to form long chains as well [3]. Since diatoms are denser than water and they normally sink under gravity, any strategy that helps to create a condition to reduce the sedimentation speed will be evolutionary advantageous.

In [9], diatom chains are modelled as nearly inextensible two-dimensional fibres with large bending resistance. Sedimentation of diatoms are studied using the immersed boundary method. It was found that the speed of sedimentation is affected by the length as well as the orientation [8] for an isolated fibre or a group of fibres with relative large separation distance. On the other hand, when the separation distance is small, sedimentation speed is greatly enhanced, due to hydrodynamic interaction. It was also found that orientation of these fibres becomes less a factor under a shear flow. While these findings are informative, it is not clear what determines the separation distance among diatoms in an environment where planktons could grow. In this paper, we develop an immersed boundary method to investigate the dynamical process of diatom growth and sedimentation, where the separation distance among diatoms is a not a pre-determined parameter.

The main feature of our immersed boundary method is that the length of the immersed structure is under active control. First of all, the diatom chain element is nearly inextensible without growth, which is approximated by a nonlinear strain-hardening spring. Secondly, the growth of diatoms is modelled by adding extra element to the diatom chain. Finally, when the chain breaks, a repulsive force among diatom chains is imposed to modelled the thick setae structures found in

Received by the editors March 10, 2015.
2000 *Mathematics Subject Classification.* 35R35, 49J40, 60G40.
This research was supported in part by NSERC (HH) and a Fields Institute centre for mathematical medicine postdoctoral fellowship (YHT).

some diatom species [13]. Otherwise, diatoms are allowed to move freely under gravity and the surrounding flow fields.

In Section 2, an immersed boundary formulation of Navier-Stokes equations and interfacial forces are described. A model for diatom growth and breakup is proposed in Section 3. In Section 4, we present simulations to demonstrate the effectiveness of our method. We finish our paper by a short conclusion in Section 5.

2. Mathematical model

A simple mathematical model of diatom sedimentation consists of dynamics of fluid, gravitational force, and deformation of diatoms. The corresponding immersed boundary formulation [10, 12, 16] is shown as follows.

$$\frac{\partial \boldsymbol{u}}{\partial t} + (\boldsymbol{u}\cdot\nabla)\,\boldsymbol{u} + \frac{1}{Re}\nabla p = \frac{1}{Re}\Delta\boldsymbol{u} + \frac{1}{ReCa}\boldsymbol{f}_s + \frac{1}{ReBn}\boldsymbol{f}_b + \frac{\beta}{Fr^2}\boldsymbol{f}_g, \tag{1}$$

$$\nabla\cdot\boldsymbol{u} = 0, \tag{2}$$

$$\boldsymbol{f}_s = \int_\Sigma \frac{\partial}{\partial s}\left(\sigma\boldsymbol{\tau}\right)\delta\left(\boldsymbol{x}-\boldsymbol{X}\right)\,ds, \tag{3}$$

$$\boldsymbol{f}_b = \int_\Sigma \frac{\partial^2}{\partial s^2}\left(b\frac{\partial\boldsymbol{\tau}}{\partial s}\right)\delta\left(\boldsymbol{x}-\boldsymbol{X}\right)\,ds, \tag{4}$$

$$\boldsymbol{f}_g = \int_\Sigma \begin{pmatrix} 0 \\ -1 \end{pmatrix}\delta\left(\boldsymbol{x}-\boldsymbol{X}\right)\,ds, \tag{5}$$

$$\frac{\partial \boldsymbol{X}}{\partial t} = \boldsymbol{U}(s,t) = \int_\Omega \boldsymbol{u}(\boldsymbol{x},t)\delta\left(\boldsymbol{x}-\boldsymbol{X}\right)\,d\boldsymbol{x}, \tag{6}$$

where Reynolds number Re represents the ratio of fluid inertia to viscous stress, capillary number Ca and Bn respectively describe the strength of interfacial tension and bending stiffness. The bending stiffness is simply a constant during diatoms sedimentation, while the interfacial tension is described as a nonlinear strain-hardening spring of the form $\sigma = \left(\sigma_l + \sigma_n {\Delta S_\alpha}^2\right)\Delta S_\alpha$, where σ_l and σ_n are respectively linear and nonlinear constants controlling inextensible strength, and ΔS_α is the difference of stretching factor. The Froude number Fr is the ratio of fluid inertia to gravitational force, and dimensionless number $\beta = \Delta\rho D$ is the relative density difference scaled by the diatom diameter (relative to its length). The diatom chain is parameterized as a function $\boldsymbol{X}(t,\alpha)$. Equations (3)-(5) distribute interfacial forces (on Σ) to body forces (on Ω) through Dirac delta function, while Equation (6) shows that the interfaces are carried by the fluid flow with interfacial velocity $\boldsymbol{U}$ which is interpolated using bulk fluid velocity $\boldsymbol{u}$.

3. Growth and breakup

Growth and breakup mechanisms play essential roles in life cycle of diatoms [5, 7]. Both affect the sedimentation speed such that diatoms can adapt the change of environments [2, 4]. Physically, growth mainly involves in the distribution of nutrition in sea water [2, 6, 15], which can be represented by the concept of concentration (weight per volume). Mathematically, the nutrition concentration can be simplified as $c(t,\boldsymbol{x})$, a function of time and space. The corresponding numerical methods to handle concentration issues can be found in [10, 11].

With the definition of concentration, the growth rate is intuitively a concentration dependent function, $v_g(c(t,\boldsymbol{X}))$. Here, an interpolation process to obtain the effective concentration $c(t,\boldsymbol{X})$ on interfaces is essential. Moreover, the average growth rate of a single diatom and corresponding growth of a diatom chain $L(t)$ in

a time period t are defined separately as

$$\bar{v}_g(t) = \frac{1}{|\Sigma|}\int_\Sigma v_g(c(t,\boldsymbol{X}))ds, \qquad L_g(t) = \int_0^t \bar{v}_g(t')dt'. \tag{7}$$

Bending energy builds up inside diatom chains as they grow, due to the deformation caused by the fluid flow. A realistic model for the breakup of a diatom chain should release the bending energy gradually, perhaps due to the weakening of the stiffness. In this paper, we focus on how breakup of the chains affects overall diatom sedimentation rate. Therefore, we use a simple approach by removing a small segment after the chain reaches a critical length, which results in a sudden release of bending energy at the moment of breakups.

When a diatom chain breaks up, most species of diatoms have setae surrounding the bodies, which prevents entangling of the chains and ensure a minimum distance among them. Here, we introduce a potential function ϕ to mimic seta mechanism

$$\phi(\boldsymbol{X},\boldsymbol{X}') = \begin{cases} \epsilon\left(r^{-l} - R_M^{-l}\right), & r \le R_M \\ 0, & r > R_M \end{cases} \tag{8}$$

where ϵ is the strength of the repulsive force, $r = |\boldsymbol{X} - \boldsymbol{X}'|$ is the distance between addresses of markers $\boldsymbol{X}$ and $\boldsymbol{X}'$, and R_M is the cutoff distance. The corresponding repulsive force is given by

$$\boldsymbol{f}_r = \int_\Sigma \boldsymbol{F}_r\,\delta\left(\boldsymbol{x} - \boldsymbol{X}\right)ds, \quad \boldsymbol{F}_r = -\nabla\phi. \tag{9}$$

Numerical treatments for the growth and breakup of chains can be complicated and challenging. For simplicity, we focus on the effects of growth speed and breakup option, and assume that there is abundant of nutrition and $\bar{v}_g$ is a constant. Let Δt be the time step size, and Δs (typically around $0.5h$, h is the mesh spacing of Eulerian coordinates) be the initially uniform mesh spacing of Lagrangian coordinates. The growth of a chain at each time step is simply $\Delta L = \bar{v}_g\Delta t$. A marker point is added in the tangential direction of each tip whenever $\sum_k \Delta L > \Delta s$, where k is the counter of time steps. Furthermore, we denote L_0 as the original length of a chain with M_0 pieces of Δs and the breakup is done by directly removing a small piece of a chain when it grows up to $mL_0 + 2(m-1)\Delta s$ and breaks up into m chains with length L_0 for each piece.

To compute repulsive forces, distance searching between a pair of markers among diatom chains can be time consuming. To reduce computation cost, an effective distance $R_M = 2h$ is used. Instead of searching marker by marker among the diatom chains, we take the advantage of indices searching process in IB method, which uses a cell-to-cell checking process. For instance, the mth marker of chain n, $\boldsymbol{X}_{m,n}$, belongs to its mother cell (i,j) which encloses at least one coordinate (m,n) (each cell may enclose either no marker or more than one marker). Searching any index other than n in cell (i,j) and its vicinity cells gives the potential of marker $\boldsymbol{X}_{m,n}$ and simultaneously counts part of potential for close-by markers (other than chain n).

4. Numerical simulations

In this section, numerical studies on sedimentation speed of diatom chains will be shown in terms of chain orientation, growth speed, and breakup option. Corresponding numerical setup is based on [9], the characteristic length is 10^{-3} m, and the characteristic velocity is 2×10^{-5} m/s. Water density and viscosity are 1000 kg/m^3 and 0.001 Pa.s, respectively. The density of diatoms is 1100 kg/m^3 of chain

diameter 10^{-5} mm, and its bending rigidity is 10^{-13} Nm. A computational domain $\Omega = [-1, 1] \times [-3.2, 0]$ is considered for all tests, except the study of domain size issue. For simplicity, we impose periodic boundary condition in x-direction and Neumann boundary conditions (zero shear) at $y = -3.2$ and $y = 0$. The mesh spacing h of Eulerian coordinates is 0.02, while the time spacing $\Delta t = 0.1h$ is small enough for numerical stability in all cases.

4.1. Single chain growth and breakup. As we know, a single chain sedimentation speed correlates to both orientation and length of a chain, and the average sinking velocity of a group of diatom chains is significantly larger than a single chain [9]. Figure 1(a) shows evolution of sedimentation speed of a single chain (length L_0) with orientation variation, the performance matches the conclusion in [8, 9] well, i.e., the larger the orientation angle (within 0 for horizontal to $\pi/2$ for vertical orientations) the greater the sedimentation speed.

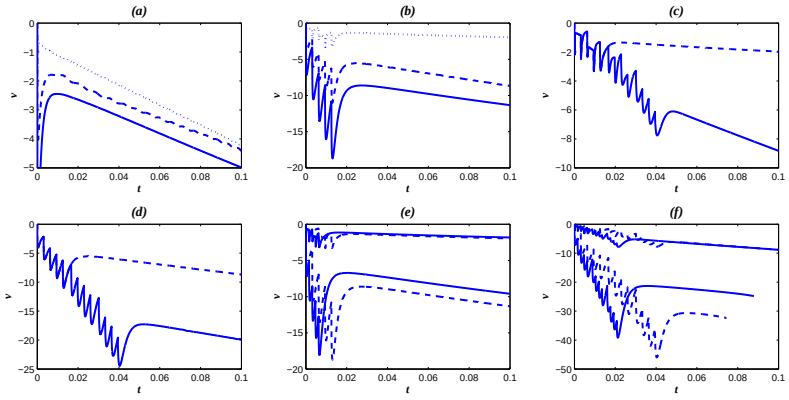

FIGURE 1. Sedimentation speed of a single chain. (a) A chain of length L_0 under variation of orientation angles $\theta = 0$ (dot), $\pi/4$ (dash), and $\pi/2$ (solid). (b) A chain grows up to length $2L_0$ with chain growth rate $\bar{v}_g = 4$ under variation of orientation angles $\theta = 0$ (dot), $\pi/4$ (dash), and $\pi/2$ (solid). (c) A chain grows up to $2L_0$ (dash) and $4L_0$ (solid) under the same growth rate $\bar{v}_g = 4$ and orientation angle $\theta = 0$. (d) A chain grows up to $2L_0$ (dash) and $4L_0$ (solid) under the same growth rate $\bar{v}_g = 4$ and orientation angle $\theta = \pi/4$. (e) Effect of chain growth rates $\bar{v}_g = 4$ (dash) and $\bar{v}_g = 8$ (solid): $2L_0$ growth with orientation angle $\theta = 0$ and $\theta = \pi/2$. (f) Effect of chain growth rates $\bar{v}_g = 4$ (dash) and $\bar{v}_g = 8$ (solid): $4L_0$ growth with orientation angles $\theta = 0$ and $\theta = \pi/2$.

Instead of assigning fixed fiber lengths initially, here, we set diatom growth rate $\bar{v}_g$, and examine sedimentation speed of a single chain with orientation angles $\theta = 0$, $\pi/4$, and $\pi/2$. When the length of a diatom reaches $2L_0$, the resulting sedimentation speed in Figure 1(b) is consistent to Figure 1(a). Figure 1(c) displays sedimentation speeds of different growth length with the same orientation angle $\theta = 0$, and we see a greater sinking velocity for a longer chain. Similar tendency occurs when the orientation angle is changed to $\theta = \pi/4$, see Figure 1(d). Next, we examine the effect of growth speed on sinking velocity. In Figure 1(e), a chain

grows up to $2L_0$, and the top group lines and bottom group lines respectively have $\theta = 0$ and $\theta = \pi/2$. Both dash lines have $\bar{v}_g = 4$, while solid lines have $\bar{v}_g = 8$. Similarly, cases of a chain growing up to $4L_0$ are performed in Figure 1(f). Notice that the oscillation of velocity profile in each case occurs at chain growth moment, an extra small piece of diatom is suddenly added such that the chain sinking velocity is rapidly increased, meanwhile, the fluid feels this extra piece of moving obstacle and viscous stress drags this rapid movement back to form one of valleys in an oscillatory velocity profile.

In the following, we consider the breakup mechanism during chain growth process. Figure 2(a) shows three cases of evolution of sedimentation speed. A horizontal chain with growth speed $\bar{v}_g = 4$ and without breakup which grows up to $2L_0$ is shown as the dash line, while the solid line represents a case under the same conditions except breaking up into two pieces. As shown by the solid line, a positive overshot appears right after breaking, this is due to the release of bending energy. During chain sedimentation, deformation of chain represents a stored bending energy in a chain, however, breakup action divides equally the bending energy such that each portion of the energy suddenly becomes strong to a shorter chain (around L_0) and induces opposite effect to sedimentation. Similar phenomenon is observed when the growth rate increases to $\bar{v}_g = 8$, see dash-dot line, here, a peak shows up earlier and then acts in the same way as solid line. Figures 2(d) and (e) display the vorticity profile of solid line before and after breakup moment, respectively. Two vortices surround each tip of the chain before breakup, while four more vortices are produced at the breakup gap due to the access of fluid across the chain.

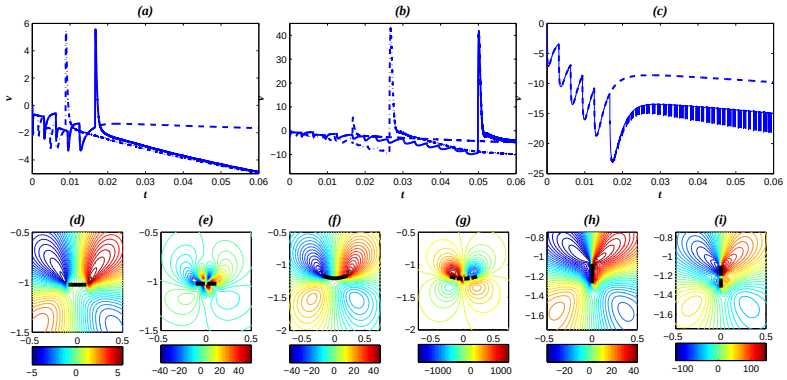

FIGURE 2. (a) A horizontal chain with $2L_0$ growth: $\bar{v}_g = 4$ without breakup (dash), $\bar{v}_g = 4$ breakup (solid), and $\bar{v}_g = 8$ breakup (dash-dot). (b) A horizontal chain with $4L_0$ growth: $\bar{v}_g = 4$ without breakup (dash), $\bar{v}_g = 4$ breakup (solid), and $\bar{v}_g = 8$ breakup (dash-dot). (c) A vertical chain with $2L_0$ growth in $\bar{v}_g = 4$: without breakup (dash), and breakup (solid). (d) Vorticity contour of solid line in (a) before breakup. (e) Vorticity contour of solid line in (a) after breakup. (f) Vorticity contour of solid line in (b) before breakup. (g) Vorticity contour of solid line in (b) after breakup. (h) Vorticity contour of solid line in (c) before breakup. (i) Vorticity contour of solid line in (c) after breakup.

Similarly, sedimentation speeds of a chain with $4L_0$ growth are shown in 2(b), and the corresponding vorticity contours of solid line case before and after breakup are separately illustrated in figures 2(f) and (g). Intuitively, there are more bending energy storing in a chain of length $4L_0$, and we observe large deformation of the chain before breakup, see (f). After breakup, larger bending energy creates a higher peak in evolution of sinking velocity (solid line in 2(b)) than in 2(a), and vortices are produced at breakup gaps, see (g). A case with growth rate $\bar{v}_g = 8$ schedules an earlier peak moment which is shown as dash-dot line, and enhances the sinking velocity a little bit than the solid line. In 2(c), a vertical chain with growth speed $\bar{v}_g = 4$ is settled to grows up to $2L_0$, dash line shows evolution of the sinking velocity without breakup mechanism, while the solid line performs the result with breakup consideration. The corresponding vorticity contour profiles can be found in 2(h) and (i). Notice that a peak with positive velocity does not exist at the breakup moment due to the lack of chain deformation (vertical orientation is parallel to the sedimentation direction).

4.2. Multiple chain growth and breakup. As described in the previous section, a nonlinear spring model is used to approximate the nearly inextensibility of diatoms. Numerical tests are carried out to investigate the effects of stiffness coefficient and evolutions of relative error of diatom length are given in Figure 3. In the tests, the linear component is fixed as $\sigma_l = 1$. We compare the effects of nonlinear spring coefficient on total extension using a horizontally placed diatom with rest length $4L_0$. We find that nonlinear strain is negligible until $\sigma_n \geq 1000$. In all cases, the relative extension stays within 1%, as shown in Figure 3(a). A subplot inserted in the plot shows a 30% length reduction without imposing the spring force. Similar results are obtained for a vertical diatom performs, cf. Figure 3(b), where a 16% reduction of length occurs without the spring force. Figure 3(c) illustrates that a linear spring maintains inextensibility better for a stiff diatom than for a softer diatom in Fig. 4.

Next, we present the simulations of a system with multiple diatom chains. We examine the average sinking velocity for several cases: (I) without growth and breakup options (dot line), (II) grows up-to twice of original length without breakup (dash line), and (III) breakup after growing up-to twice of initial length (solid line).

Figure 4(a) shows evolution of sedimentation speeds of a 4-chain group. For comparison purpose, the sedimentation rate for an individual chain in the 4-chain group (dash line) and a vertical single chain (solid line) are plotted in the subplot. The vorticity contour before the breaking up of the chains is illustrated in (d), while (e) shows the vorticity after the breakup. Similar patterns of 8-chain group are shown in Figures 4(b), (f), and (g). Results for 16-chain group are given in Figures 4(c), (h), and (i). In Figures 4(a)-(c). We observe that the average sedimentation speed of a group of chains is proportional to the number of chains. In each figure, a group with growth chains has a greater sedimentation speed than a group without growth, while breakup of the chains enhances the sinking rate further.

In Figure 5(a), we examine sedimentation speed of 16-chain group under different dimensionless bending rigidity: $b = 1.0$ (dot line), $b = 0.1$ (dash line), and $b = 0.01$ (solid line). As expected, softer diatoms sinks faster as deformation reduces resistance from the surrounding fluid. Two snapshots of vorticity contours before and after breakup are shown in Figures 5(b) and (c), both showing significant deformation in diatoms.

An important issue from application point of view is the effect of diatom density on sedimentation rate. A related computational issue is the effect of the boundary

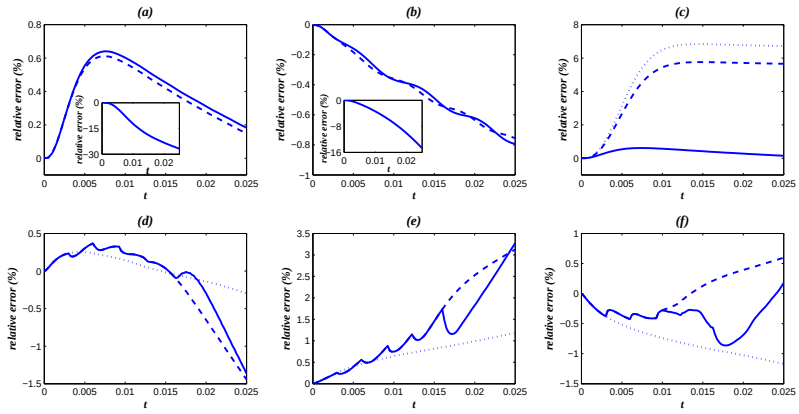

FIGURE 3. Evolution of relative error (%) of total length with fixed linear spring constant $\sigma_l = 1$: (a) A horizontal placed diatom of length $4L_0$ with extra nonlinear spring constraints, $\sigma_n = 0$ (dash), and $\sigma_n = 1000$ (solid). For comparison purpose, the result for the same diatom without the spring force is also included as the subplot; (b) A vertical diatom of length $4L_0$ with extra nonlinear spring constraints, $\sigma_n = 0$ (dash), and $\sigma_n = 1000$ (solid); (c) Linear spring for diatom rigidities $b = 0.01$ (dot), $b = 0.1$ (dash), and $b = 1.0$ (solid); (d) Relative extension for the 4-chain group in Figure 4(a), without growth and breakup (dot), growth only (dash), and breakup after growth (solid); (e) Relative extension for the 8-chain group in Figure 4(b), without growth and breakup (dot), growth only (dash), and breakup after growth (solid); (d) Relative extension for the 16-chain group in Figure 4(c), without growth and breakup (dot), growth only (dash), and breakup after growth (solid).

condition. For sedimentation problem, when viscous dissipation is sufficiently large, a terminal sinking speed is reached. On the other hand, when viscous dissipation is not sufficient to balance the potential energy, falling objects will accelerate. In our setup (with periodic boundary condition in the horizontal direction), the density of diatoms is determined by two parameters: the number of diatom chains in the periodic box and the length of the period. In Figure 4, we have investigated the effect of diatom numbers (density) among other things. And it was clear that steady sedimentation only occurs for the four-chain (low density) case.

The effect of domain size and boundary conditions on the sedimentation is illustrated in Figure 6. In Figure 6(a), evolution of sedimentation speed of a 16-chain group is shown in dot line as a reference (also see solid line of Figure 4(c) in detail). Dash line shows a result of replacing Neumann boundary condition in y-direction by periodic boundary condition, and the difference between this case and the one with Neumann condition in the y-direction is small. Keeping Neumann boundary condition and increasing the domain size in the y-direction results in a slower sedimentation acceleration, as shown by the dash-dot line. Acceleration is reduced further (as shown by the solid line) when the domain size in the y-direction is

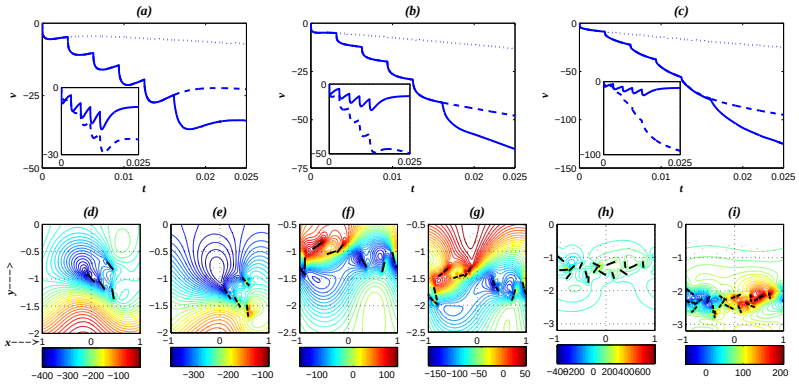

FIGURE 4. Comparison of sedimentation speed under growth and breakup effects. (a) Four chains group: without growth and breakup (dot), growth only (dash), and breakup after growth (solid). (b) Eight chains group: without growth and breakup (dot), growth only (dash), and breakup after growth (solid). (c) Sixteen chains group: without growth and breakup (dot), growth only (dash), and breakup after growth (solid). (d) Vorticity contour of solid line in (a) before breakup. (e) Vorticity contour of solid line in (a) at $t = 0.025$. (f) Vorticity contour of solid line in (b) before breakup. (g) Vorticity contour of solid line in (b) at $t = 0.025$. (h) Vorticity contour of solid line in (c) before breakup. (i) Vorticity contour of solid line in (c) at $t = 0.025$.

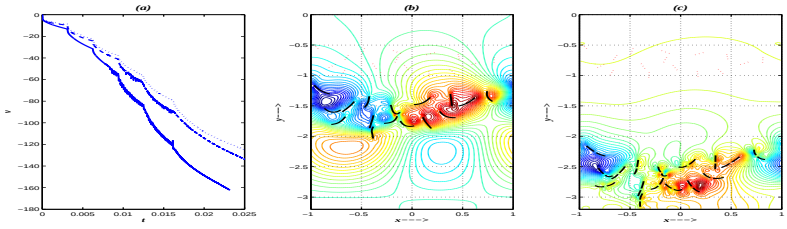

FIGURE 5. (a) Comparison of sedimentation speed of 16-chain group under different bending rigidity: $b = 1.0$ (dot), $b = 0.1$ (dash), and $b = 0.01$ (solid). (b) Vorticity contour of 16-chain group with $b = 0.01$ before breakup. (c) Vorticity contour of 16-chain group with $b = 0.01$ at $t = 0.023$.

increased by four-fold. This indicates that the size in the y-direction is not the dominant factor even though it has an effect in the sedimentation behaviour.

Figure 6(b) demonstrates the effect of domain size in the x-direction on sedimentation speed. Results for $L_x = 3$ (dash line), $L_x = 4$ (dash-dot line), and $L_x = 6.0$ (solid line) show that steady sedimentation has established for these cases. The corresponding vorticity contour at $t = 0.025$ are presented in (c)-(e), respectively. Clearly, larger domain sizes in the x-direction (indicating lower diatom density due

to the periodicity in the x-direction) weaken hydrodynamic interaction (and increase viscous dissipation). For comparison purposes, in Figure 6(b), we have also shown the case for $L_x = 2$ (dot, also shown by the sold line in Figure 4(c)), and the corresponding vorticity contour at $t = 0.025$ can be found in Figure 4(i). The results suggest that for $L_x \geq 3$, viscous dissipation is sufficiently strong for the group of diatoms to reach steady sedimentation while this is not the case for $L_x = 2$.

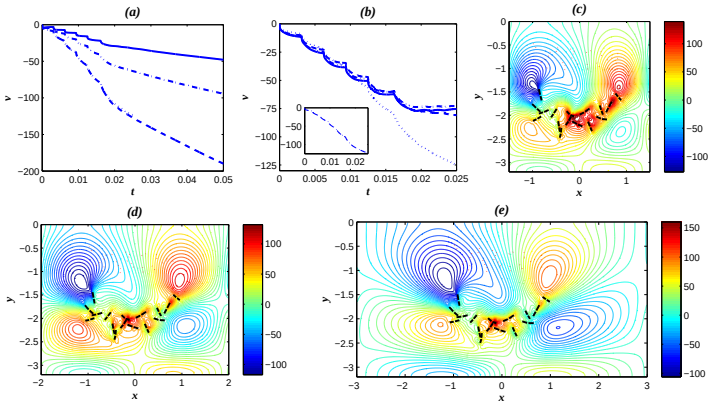

FIGURE 6. (a) Evolution of 16-chain sedimentation speed in domain of different conditions in y-direction: Neumann boundary condition with $L_y = 3.2$ (dot), periodic boundary condition with $L_y = 3.2$ (dash), Neumann boundary condition with $L_y = 6.4$ (dash-dot), and Neumann boundary condition with $L_y = 12.8$ (solid). (b) Evolution of 16-chain sedimentation speed in domain of different periodic widths: $L_x = 2.0$ (dot), 3.0 (dash), 4.0 (dash-dot), and 6.0 (solid). (c) Vorticity contour of $L_x = 3.0$ case at $t = 0.025$. (d) Vorticity contour of $L_x = 4.0$ case at $t = 0.025$. (e) Vorticity contour of $L_x = 6.0$ case at $t = 0.025$.

5. Conclusion

In this paper, we presented an immersed boundary method for studying plankton (diatom) sedimentation with growth and breakup mechanisms. In reality, diatom growth rate is a nutrition (concentration) dependent function. In order to simplify our model and maintain computational efficiency, we assume the rate to be a constant, much greater than the actual value. Once diatom growth rate is determined, the instantaneous total growth of a chain is evaluated by an average rate within a time period. Computationally, we take advantage of the IB method framework and the growth of a chain is handled by adding additional markers at the two ends of the chain, while the breakup mechanism is modelled by removing a small piece of the chain. An efficient cell-cell searching algorithm replaces a regular marker-marker searching to calculate potential of each marker.

Our simulations show that diatom growth increases sedimentation speed, which is proportional to diatom length, while the growth rate has minor effects on diatom sedimentation. Both diatom growth and breakup enhance the average sedimentation speed, and the sinking rate is proportional to the number of diatoms in the chain. In addition, our results show that diatoms with smaller bending rigidities

sink faster, which are at a disadvantage compared to the ones with a larger bending rigidity.

Even though we focused on diatom sedimentation in this paper, the method developed here could be used for studying other problems as well. For example, it can be modified to investigate the effect of fibre aggregation on sedimentation by reversing the breakup process, or the dynamics of fibres with local interactions, either under gravity or driven by other forces.

References

[1] L. Botes, Phytoplankton Identification Catalogue Saldanha Bay, South Africa, April 2001. GloBallast Monograph Series No. 7. IMO London (2003).
[2] P. Castro and M.E. Huber, Marine biology, 5th Ed., 312-320 (2005).
[3] V. Cassie, Marine Plankton Diatoms, Tuatara 7(3), (1959)
[4] K.L. Denman and A.E. Gargett, Biological/physical interactions in the upper ocean: the role of vertical and small scale transport processes. Ann. Rev. Fluid Mech. 27, 225-255 (1995).
[5] J.W. Dippner, A Lagrangian model of phytoplankton growth dynamics for the Northern Adriatic Sea. Cont. Shelf Res. 13, 331-355 (1993).
[6] P.G. Falkowski and J.A. Raven, Aquatic photosynthesis. Princeton University Press, Princeton (2007).
[7] P.J.S. Franks, J.S. Wroblewski and G.R. Flierl, Prediction of phytoplankton growth in response to the frictional decay of warm-core ring. J. Geophys. Res. 91C, 603-610 (1986).
[8] D.P. Holland, Sinking rates of phytoplankton filaments orientated at different angles: theory and physical model. J. Plankton Res. 32, 1327-1336 (2010).
[9] P. Huang, Mathematical modeling of phytoplankton sedimentation. MSc Dissertation, York University (2012).
[10] M.-C. Lai, Y.-H. Tseng and H. Huang, An immersed boundary method for interfacial flow with insoluble surfactant. J. Comput. Phys. 227, 7279-7293 (2008).
[11] M. Muradoglu and G. Tryggvason, A front-tracking method for computations of interfacial flows with soluble surfactants. J. Comput. Phys. 227, 2238-2262 (2008).
[12] C.S. Peskin, The immersed boundary method. Acta Numer. 11, 139 (2002).
[13] J.D. Pickett-Heaps, Cell Division and Morphogenesis of the Centric Diatom Chaetoceros Decipiens (Bacillariophyceae) I. Living Cells. J. Phycol. 34, 989994 (1998).
[14] C.S. Reynolds, The Ecology of Freshwater Phytoplankton. Cambridge University Press, Cambridge (1984).
[15] M. Steinacher, F. Joos, T.L. Frolicher, L. Bopp, P. Cadule, V. Cocco, S.C. Doney, M. Gehlen, K. Lindsay, J.K. Moore, B. Schneider and J. Segschneider, Projected 21st century decrease in marine productivity: a multi-model analysis. Biogeosciences 7, 979-1005 (2010).
[16] J.M. Stockie and S.I. Greeny, Simulating the motion of flexible pulp fibres using the immersed boundary method. J. Comput. Phys. 147, 147-165 (1998).

Department of Applied Mathematics, National University of Kaohsiung, Kaohsiung City 81148, Taiwan
E-mail: yhtseng@nuk.edu.tw
URL: http://140.127.223.1/yuhautseng/index.htm

Decision Support, University Health Network (UHN), 525 University Avenue, Toronto, ON, M5G 2L3, Canada
E-mail: Ping.Huang2@uhn.ca

Department of Mathematics and Statistics, York University, Toronto, Ontario M3J 1P3, Canada
E-mail: hhuang@yorku.ca
URL: http://www.math.yorku.ca/Who/Faculty/hhuang/menu.html